

Seeing the heat – preliminary studies of cryocrystallography using infrared imaging†

Edward H. Snell,^{a*} Russell A. Judge,^b Mike Larson^c and Mark J. van der Woerd^a

^aUSRA at NASA Laboratory for Structural Biology, Code SD46, NASA MSFC, Huntsville, AL 35812, USA, ^bUAH at NASA Laboratory for Structural Biology, Code SD46, NASA MSFC, Huntsville, AL 35812, USA, and ^cIRCameras.com, PO Box 801038, 5466 Fripp Hollow, Acworth, GA 30101, USA.
E-mail: eddie.snell@msfc.nasa.gov

As preparation for an extensive study that aims to image the cryocooling process of macromolecular crystals, the ability to thermally image solid objects and liquids at temperatures far below 273 K is demonstrated. In the case of a large lysozyme crystal ($1.0 \times 0.7 \times 0.2$ mm), qualitative measurements show the cooling process to take about 0.6 s with the cooling taking place in a wave starting from the face of the crystal nearest to the origin of the cryostream and ending at the point furthest away from the origin. Annealing of this lysozyme crystal, cooled under good cryoprotectant conditions, shows that cold striations form perpendicular to the cooling stream. These striations become more pronounced after successive annealing. Cryocooling of a non-cryoprotected crystal of glucose isomerase displayed an ‘S-shaped’ cold front wave traveling across the sample. These preliminary results are qualitative but show the power of infrared imaging as a new tool for fundamental and practical cryocrystallography studies.

Keywords: macromolecular cryocrystallography; thermal imaging; infrared camera.

1. Introduction

Rapid cooling or cryopreservation of macromolecular crystals is routinely used for structural X-ray data collection. Cryopreservation decreases the thermal scatter and radiation damage, resulting in increased resolution and completeness of the data. The objective of correctly cooling a macromolecular crystal is to preserve the crystal and the liquid around it in a glass phase and to avoid ice formation. In order to avoid crystalline ice, Weik *et al.* (2001) provided quantitative data for the upper limit for the storage and handling of a crystal at 155 K. The methods and techniques of cryocooling have been well studied experimentally (Garman, 1999; Garman & Schneider, 1997; Rodgers, 1997). Teng & Moffat (1998) and Walker *et al.* (1998) have investigated cooling rates in different media using thermocouples. In the Teng & Moffat (1998) study, the cryoloop was made of the thermocouple with two different volumes (0.2 mm^3 and 0.8 mm^3) of test buffer for quantifying a typical fast and slow cooling investigated with nitrogen gas, helium gas, liquid nitrogen and liquid propane. The cooling rates varied from $\sim 50 \text{ K s}^{-1}$ to 700 K s^{-1} depending on the volume of the sample, the cooling agent and the temperature at the time of measurement. Walker *et al.* (1998) used a bare thermocouple and one coated with a 0.25 mm layer of silicone rubber cement to simulate a crystal. In these two studies, the experimental setup gave a single measurement for the whole system and provided temporal but

no spatial resolution. Different results were obtained in each study; however, neither looked directly at a crystal. We are using thermal imaging with an infrared (IR) camera, which is a non-invasive technique that allows for observation of a crystal at various temperatures.

All objects above 0 K emit thermal energy. The emission and absorption of radiation is usually defined with reference to a perfect emitter/absorber, termed a blackbody. The spectrum of radiation emitted by a blackbody, as energy density per unit time per unit wavelength, is given by Planck’s radiation law:

$$E(\lambda, T) = (2\pi hc^2)/\{\lambda^5[\exp(hc/\lambda kT) - 1]\} \quad (1)$$

where λ is the wavelength, c is the speed of light, k is the Boltzmann constant, h is Planck’s constant and T is the temperature in kelvin. Fig. 1 shows the spectra for a blackbody at various temperatures from ambient down to typical cryocooling temperatures of 100 K. The graph is enlarged in the region of sensitivity of the IR camera used. In practice, objects are not perfect blackbody radiators, and therefore energy is not perfectly emitted or absorbed. To reflect this non-ideal behavior, the blackbody radiation spectra seen in Fig. 1 are commonly corrected by the emissivity: the ratio of radiation emitted by a surface to the radiation emitted by a blackbody under the same conditions. Emissivity is a function of temperature and wavelength. Some typical emissivity values are 0.96 for distilled water at 293 K and 0.95 for smooth ice, 0.98 for frost crystals and 0.85 for snow, all at 263 K (Hudson, 1969). To date there are no reliable emissivity values available for macromolecular crystals.

A camera sensitive to IR radiation measures the intensity of the radiation at a given wavelength or in a wavelength band. This measured intensity relates to the temperature of the object under study by Planck’s law (1), taking into account the characteristics of the camera. The temperature response of the camera is non-linear and is corrected for by imaging a hot and a cold object, then applying a response function to the data. Once the non-linearity correction has been made, calibration with objects of known temperature allows for conversion of the intensity of radiation, measured in counts, to temperature. The atmosphere reduces the transmitted IR energy by air absorption (e.g. by water vapor, carbon dioxide and ozone) and by scattering. There are, however, several windows in the IR spectrum where the absorption and scattering are minimized. These windows are termed the near- ($0.8\text{--}1.1 \mu\text{m}$), mid- ($3\text{--}5 \mu\text{m}$) and far-IR ($8\text{--}12 \mu\text{m}$). The energy density (Fig. 1) at the temperature range under study here is greater in the mid-IR range than the near-IR range. The mid-IR range also has a greater response to change in temperature than the far-IR range. For this reason we use an IR camera sensitive to the mid-IR range. In this paper, we describe the first use of a thermal camera to observe the cooling of glycerol, a cryoprotected lysozyme crystal and an unprotected glucose isomerase crystal, all mounted in nylon loops.

2. Experimental

An Oxford Cryostream 600 was set up on an optical table and used with a nitrogen gas stream measured at the tip of the nozzle to be 100 K. The cryostream uses an outer dry air stream to surround the inner cold nitrogen-gas flow, which has a linear speed of 0.44 m s^{-1} . An Indigo Systems Merlin mid-range IR camera was used for imaging. This uses an indium antimonide (InSb) type detector with a spectral range of $1.0\text{--}5.4 \mu\text{m}$ cooled by a Sterling engine to an operating temperature of 77 K. The camera was equipped with a $4\times$ magnification IR microscope lens and positioned to observe a pin mounted on a goniometer head in the middle of the coldstream. The end of the lens was approximately 20 mm from the center of the

† Presented at the ‘Second International Workshop on Radiation Damage to Crystalline Biological Samples’ held at Advanced Photon Source, Chicago, USA, in December 2001.

radiation damage workshop

coldstream. The detector has 300×256 pixels, each imaging $7.5 \times 7.5 \mu\text{m}$ with the magnification used. Images from the camera were recorded using both video and digital capture with a maximum frame rate of 60 Hz. Typically, IR cameras are used to image hot scenes, *i.e.* objects above ambient temperature. For that application, a

non-uniformity correction is applied by imaging an ambient (low) temperature and a higher point. In our case, the high temperature is ambient and the non-uniformity correction is achieved by imaging a black metal plate cooled in a 193 K freezer. The measurements, acquired by the program *TALON*, were made in terms of intensity

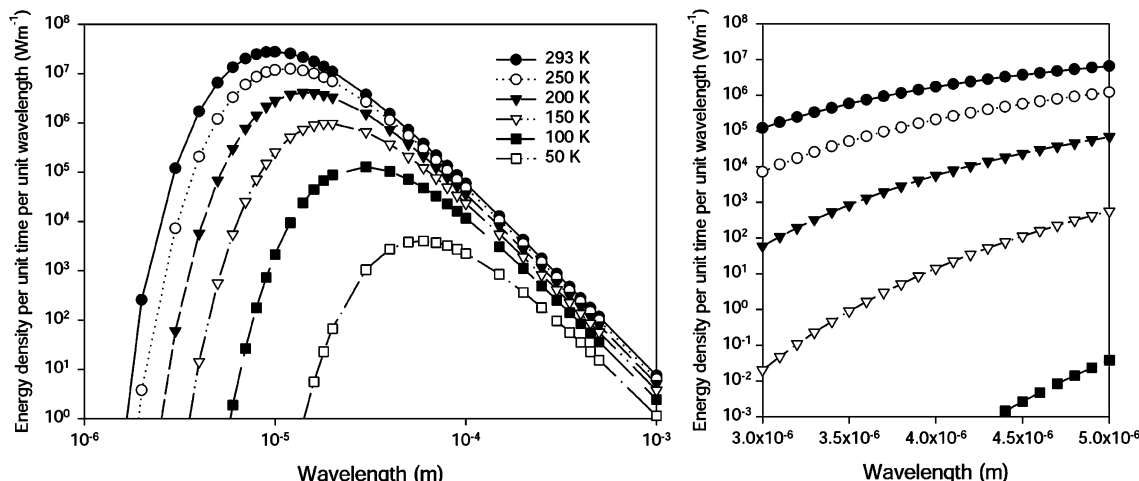


Figure 1

Graph showing an IR spectrum of blackbody-radiation energy density for temperatures applicable to cryocrystallography. The entire IR spectrum is shown with an enlargement illustrating the bandpass of the IR camera used. Integrating under the graph gives the power (W m^{-2}).

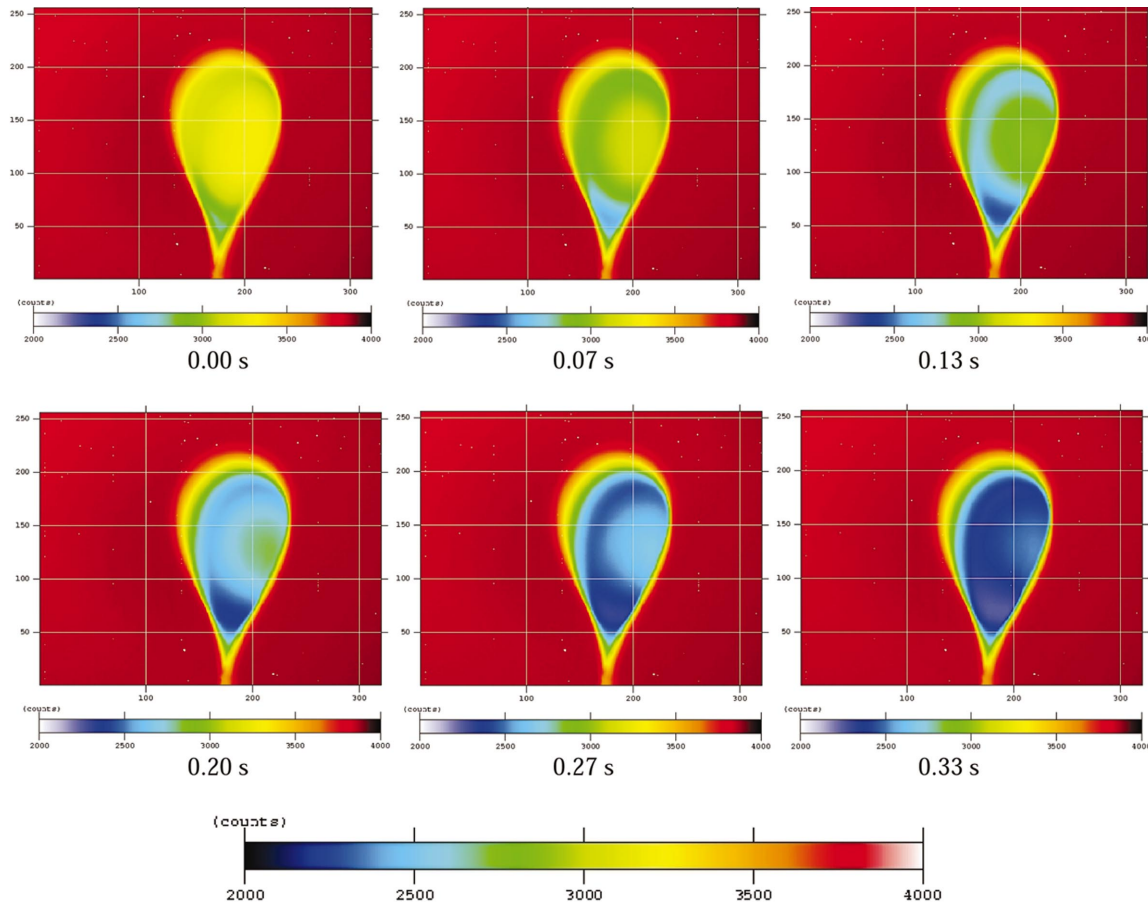
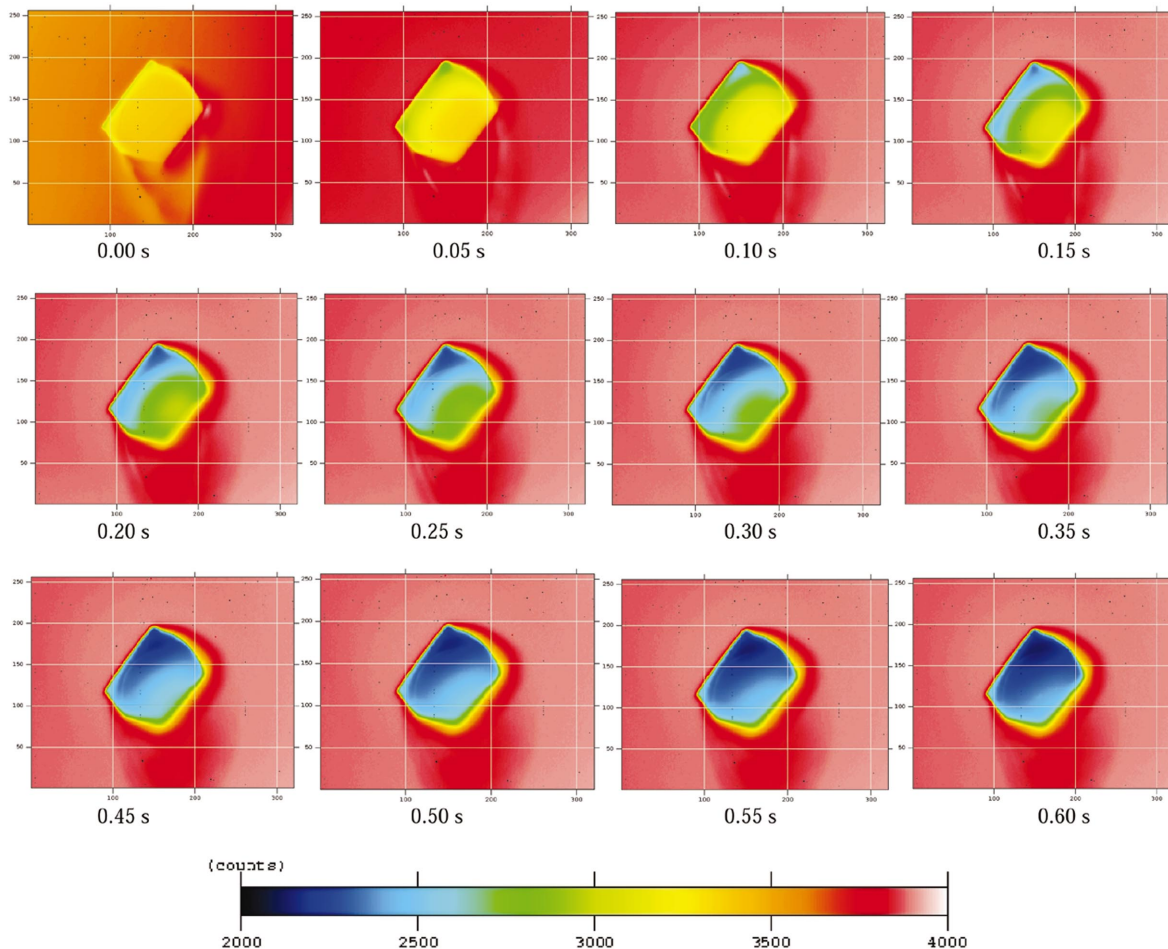
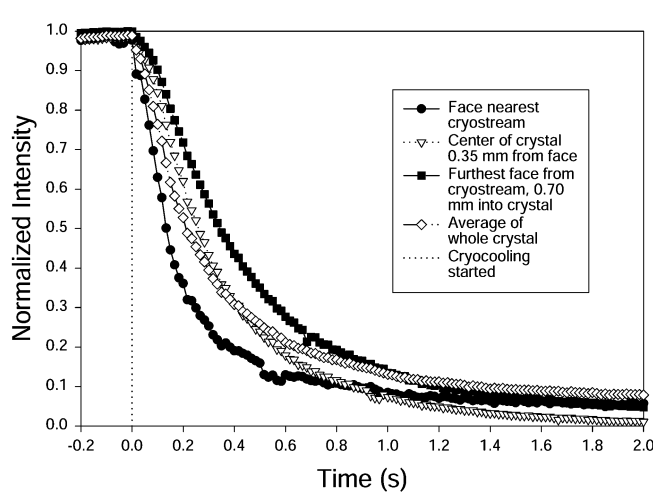


Figure 2

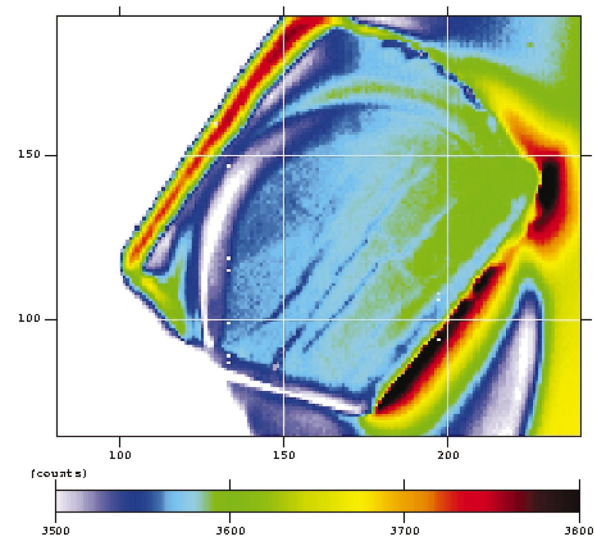
Glycerol in a cryoloop imaged with the IR camera during cooling. The time starts when the coldstream is unblocked. The loop is 0.75 mm in the horizontal plane and is positioned perpendicular to the camera but parallel to the nitrogen stream. Every fourth image is shown in this series. The image is false colored with blue being cold and red hot. The nitrogen stream is incident on the loop in the top left of the picture at an approximate 30° down angle. Overlaid on this image and subsequent images is a grid showing the pixel numbers for sizing purpose. Each pixel at this magnification is $7.5 \times 7.5 \mu\text{m}$.

**Figure 3**

A lysozyme crystal that is cryocooled in a 100 K gas stream identical to that in Fig. 2. The background is slightly cooler in the first two images because of cooling effects of the diverted cold gas stream. Every third image in the data set is shown. The images are false colored on the same scale as Fig. 2. The crystal sits on the loop, which is positioned behind the crystal in these images.

**Figure 4**

Plot of intensity at the crystal edge nearest the coldstream, the center of the crystal and the edge furthest from the cryostream for the lysozyme crystal shown in Fig. 3. Each intensity value is calculated from the average of an 11×11 pixel box. Also shown is the intensity averaged over the whole crystal.

**Figure 5**

The lysozyme crystal from Fig. 3 shown after tempering. Striations occur with lower intensities than the rest of the crystal. The false color scale has been chosen to accent these striations, which are not visible even with this enhanced coloring in the untempered images.

radiation damage workshop

Table 1

X-ray data collected from a cryocooled and subsequently tempered lysozyme crystal.

The numbers in parentheses represent the highest resolution shell (3.49–3.37 Å). The CCD detector was set well back, at 100 mm, to enable the observation of any reflection splitting. These settings explain the low resolution of the data.

	Unannealed	Tempered
Space group	$P4_32_12$	$P4_32_12$
Cell parameters, $a = b, c$ (Å)	78.19, 36.99	78.84, 36.88
Isotropic mosaicity (°)	0.61	0.54
Average redundancy	1.9 (1.9)	1.9 (1.8)
Linear R_{merge} (%)	2.3 (2.7)	2.4 (2.5)
Unique reflections	2499	2509
Average I/σ	31 (26)	30 (24)
Completeness (%)	72	70
Comments	No ice rings	Diffuse ice rings

values. These measurements are qualitative as a cryogenic blackbody calibration source at a temperature below 193 K was not available.

Chicken egg-white lysozyme crystals suitable for cryo cooling were grown in cryoconditions by vapor-diffusion. The reservoir contained buffer (0.1 M NaOAc, pH 4.8), 50% ethylene glycol and 0.9 M NaCl precipitant. The drop solution was made from 6 µl of protein (75 mg ml⁻¹) in buffer with 4 µl of reservoir solution. A crystal 1.0 × 0.7 × 0.2 mm in size was used for the cryoexperiment. Glucose isomerase crystals were grown using the batch method with ammonium sulfate as precipitant under conditions optimized from Dalziel (2000). A crystal 2.5 × 1.0 × 0.6 mm in size was used in the absence of a cryoprotectant. Larger crystals than those typically suitable for cryocrystallography were used in order to enhance any detail seen in the resulting images.

First, a steel alignment pin was imaged as the cryostream cooled from 293 K to 100 K, at 300 K h⁻¹, to verify that a change in intensity is indeed observed when a solid object is cooled to far below ambient temperature. The image was recorded using a video recorder. A flat brass alignment pinhole was then put in place with the cryostream incident on it. The cryostream was then warmed from 100 K to ambient 293 K, at 300 K h⁻¹. Images were digitally recorded with a frame grabber using a 0.002 s integration time at 100 K, 130 K, 170 K, 200 K and 230 K to establish the sensitivity of the camera.

The cryostream was cooled again to 100 K. To verify that a liquid and a solid glass can be observed with the IR camera, a drop of 100% glycerol was put in a 0.7–1.0 mm-diameter cryoloop (Hampton Research) then flash cooled by blocking the coldstream, placing the loop on the goniometer and unblocking the stream. Again, images were digitally recorded with an increased integration time of 0.004 s.

In a similar manner, the lysozyme crystal was then mounted in a loop and centered in the coldstream, fully visible in the IR image and in the focal point of the lens. The loop was rotated so that the crystal was perpendicular to the coldstream and digital recording started immediately before unblocking the stream. 2 s of digital data were collected at 60 Hz (one frame every 0.017 s), with 0.004 s integration time, and several minutes of video data at 30 Hz (one frame every 0.033 s). The cryostream was blocked again and the crystal imaged as it warmed up. The cryostream was unblocked and the crystal cryo-cooled again. This annealing took place *in situ* and would be more correctly termed tempering: annealing is rapid warming by removing the sample and placing it back in the original cryoprotected mother liquor. After several cycles, a still image was digitally recorded. A crystal of glucose isomerase crystal was studied in a similar way.

As a result of observations for lysozyme, X-ray data were recorded before and after annealing of the same cryocooled lysozyme crystal.

A Nonius FR591 Cu rotating-anode generator running at 47 kV and 126 mA with Osmic optics produced X-rays for a Kappa2000 CCD detector. The crystal-to-detector distance was 100 mm, and 20 images of 1° oscillations from the same starting φ (10 s exposures) were taken for each data collection. The data were indexed, integrated and reduced using the HKL2000 package (Otwinowski & Minor, 1997).

3. Results and observations

The cooling of the steel alignment pin was imaged until the cryostream reached 100 K. The image was false colored according to intensity using an automatic gain setting. At 100 K, a color gradient indicating an intensity variation was still seen across the pin, the lowest intensity toward the cryostream, the highest part directly away from the stream. Temporarily blocking the cryostream resulted in a rapid warming of the pin, which immediately cooled again once the stream was unblocked. Observation of the flat brass alignment pinhole showed fluctuations of the order of 5 counts in the intensity data between 100 K and 130 K, which we attribute to noise. A clear increase in intensity of 10 counts was seen from 130 K to 170 K, with further increasing counts with temperature. The number of counts represents the integrated number of photons in the bandpass over the integration time. The camera is sensitive to temperature differences in the brass block below 170 K at an integration time of 0.002 s.

Fig. 2 shows a time sequence of cryo cooling a 0.7–1.0 mm cryoloop filled with glycerol. The nylon forming the loop is 20 µm thick. The initial cooling takes place not at the edge nearest to the coldstream but at a point in the lower part of the loop. A cold wave proceeds from this point toward the edge and away from the direction of cooling toward the far point of the loop. The glycerol in its liquid and vitrified state could be imaged with the camera.

Fig. 3 shows a time sequence of cryo cooling a lysozyme crystal. At 0.6 s the cryo cooling is essentially complete; no significant intensity changes are observed after this time. Subsequent images show only a slight cooling of the tip of the crystal farthest from the cryostream. The background is cooler in the initial images, as the cold nitrogen gas is diverted from the image focal plane, cooling the background as the crystal is mounted. As soon as the cryostream is unblocked, the background warms and a thermal wave indicating a temperature gradient passes through the crystal traveling in the same direction as the cold gas. In each image, we measured the intensity at several distinct points in space using an 11 pixel square averaging and plotted them as a function of time elapsed (Fig. 4). The images clearly show a wave proceeding across the crystal from the initial point of cooling. Also noticeable is the loop on which the crystal is sitting. The loop is seen through the crystal and perturbs the cold wave as it passes.

The tempered crystal is illustrated in Fig. 5. Marked striations can be seen perpendicular to the coldstream with some faintly visible perpendicular links between two striations to form a mosaic structure. The color range has been narrowed relative to the other figures to show the striations more clearly. These striations are not seen in the initially cooled crystal. From these images, it is impossible to tell whether these striations are surface features, extend into the crystal or are internal. The X-ray data did not reveal significant differences in diffraction quality between the untempered and tempered crystal (see Table 1).

The cryo cooling of the glucose isomerase crystal demonstrates a more remarkable process (see Fig. 6). The cold wave travels through the crystal in an S-shaped pattern. In this case, the imaging was initiated shortly after unblocking the coldstream and the cold wave is already imaged within the crystal. The S-shaped pattern is illustrated

more clearly in Fig. 7, with a false color range chosen to accent this feature.

At ambient temperature the lysozyme crystal, the glucose isomerase crystal and the loop had an average intensity of ~ 3500 counts seen as a uniform orange/red color in the images.

4. Discussion

The IR camera discussed in this work measures intensity in counts for the radiation observed, and these counts relate to temperature, in theory, by Planck's law (1). In practice, the conversion from counts or intensity to exact temperature is accomplished by calibration of the camera with an object whose characteristics approach an ideal blackbody at at least two temperatures spanning the range of interest in the experiment. In this study of cryocooled macromolecular crystals, the lower temperature for calibration needs to be 100 K or below so the correct conversion at a temperature between 100 K and ambient can be found. At the time of the experiment, such a low-temperature blackbody was unavailable, and hence the intensities recorded cannot be reliably translated to absolute temperature.

In this study, we are most concerned with establishing whether objects in general and crystals in particular can be observed at temperatures far below room temperature. If indeed they can be observed, we will be able to study the crystals while they are cooling down and study their behavior, while cryocooled, in the X-ray beam.

As we lack the calibration function necessary, we cannot conclude that the steel alignment pin can be imaged at 100 K. However, it is significant that we observe an apparent difference between the side directly facing the coldstream and the side away from it. These data suggest that we may be able to observe temperature differences that are presumably at the basis of this phenomenon. However, the steel pin probably partly reflects energy from the environment, and since the environment was non-isotropic (for example, light mostly comes from above) the energy reflection will also be non-uniform. This experiment suggests that it may be necessary to encase an object to be observed in an isolation box, which will shield the experiment from outside thermal radiation.

The observation of the brass surface while it is slowly cooled or warmed indicates that significant differences in intensities can be observed in the range 130–170 K. Although the same limitations need to be borne in mind as in the previous experiment with the steel pin, the observed changes in intensity as a function of temperature make it unlikely that environmental factors are responsible. This experiment does not allow us to estimate the accuracy of the measurements. The emissivity of oxidized brass is low, 0.61 (Hudson, 1969), so we see a lower intensity than would be expected from a perfect blackbody.

The observation of a cryocooled drop of glycerol clearly shows the cooling process while it takes place. The background of the glycerol drop also clearly appears as 'hot' (note that the false colors in these images run from white for very few counts through red for high counts to brown/black for the highest counts). We observe what appears to be a gradient at the edge of the drop, in approximately the same shape as the nylon loop. The nature of this gradient will be discussed below. The drop was imaged with the widest part in view, which means that its thickness is non-uniform and is probably determined by a combination of the surface tension of the initially liquid glycerol and the shape of the loop. Thus, the drop is very thin at the edges and at the V-shaped area where the nylon wire meets the pin in which it is mounted. When the drop is cooled down, it is to be expected that the areas with little material will cool quickest. This is indeed observed: the edges of the drop and the V-shaped part cool rapidly and the cooling appears to progress from the outside inward.

It is noticeable from the images that the origin of the cold source is in the top-left corner: the drop appears coldest on that side.

In observing the lysozyme crystal, there are some features that are similar and some dissimilar to the glycerol drop. First, although it is visible in the images, we do not see an apparent gradient around the nylon loop. We can therefore reasonably conclude that the loop or the material it is made of is not causing the gradient observed at the edge of the glycerol drop. Furthermore, it is possible to observe the nylon loop behind the lysozyme crystal in enlarged images (see Fig. 3). This observation indicates that the IR camera registers objects behind the crystal, and therefore probably registers heat from the material composing the crystal itself. After cooling is complete, an apparent gradient continues to be present at the edge of the crystal. This gradient is steep on the face directly exposed to the coldstream and shallower on the reverse side. The gradient pattern suggests that it is related to the nitrogen flow pattern around the crystal. An explanation of the observed gradient could be that the IR energy from the background is absorbed in the gas layer immediately adjacent to the crystal surface, while more energy is transmitted to the camera as the distance from the surface increases. It is not clear without further experiments whether there is an actual temperature gradient around the crystal or if it appears that way because of the changing physical characteristics of the gas layers around the crystal. Modeling (Kazmiecza, 2002) suggests that the gradient at the rear of the crystal is real and is due to flow effects of the cold nitrogen stream. It is important to note that the nitrogen directly flowing onto the crystal from the coldstream is at a temperature of 100 K, but we do not observe this in the image, and therefore cold gas by itself appears not to be an observable phenomenon. Compared with previous thermocouple experiments (Teng & Moffat, 1998; Walker *et al.*, 1998), our experimental conditions and results appear to be closer to those of Teng & Moffat (1998). By comparing the data for the brass block, acquired with an integration time of 0.002 s, and for the lysozyme crystal, acquired with an integration time of 0.004 s, we observe an increased sensitivity of the camera with the longer integration time. More recent data (not shown) suggest that the camera is sensitive down to 130 K. The lysozyme crystal, after repeated tempering, clearly shows striations, which were induced by the thermal treatment. Given that we observe the loop behind the crystal, we cannot be sure where these striations actually occurred: on the surface, in the interior or both. The X-ray data would show an increase in mosaicity and possibly reflection splitting if these striations were symptomatic of misalignment in the crystal. This is not evident from the data (Table 1), but the effect could easily be smaller than that resolvable with the X-ray instrumentation used.

The glucose isomerase crystal, as shown in Fig. 7, shows an S-shaped cooling pattern. This pattern may occur because of the shape of the crystal and its orientation with respect to the coldstream. However, it is also possible that a suitable cryoprotectant actually enhances even cooling of the crystal. This hypothesis may be testable by analyzing mosaic spread in diffraction data as a function of crystal habit, orientation and cooling pattern.

The IR images show us both the mechanism and the time that the crystals take to cool. These are helpful in estimating the heat transfer phenomena observed. It is of particular interest for any calculation or model to know whether either heat transfer in the crystalline material or transfer from the crystal surface to the gas stream is the dominant feature. For good thermal conductors, such as metals, the heat transfer at the surface to the fluid becomes the most significant step, and temperature gradients inside the particle can be ignored for the purposes of modeling. A very small temperature gradient still exists inside the particle, but it is negligible compared with the gradient at

the particle surface. For less efficient thermal conductors, such as biological materials, the relationship between convective and conductive heat transfer becomes more complicated. The relative importance of these two heat-transfer mechanisms can be expressed in terms of the Biot number, Bi , where $\text{Bi} = hR/K$, with h the average convective heat-transfer coefficient, R the radius or characteristic half length of the particle, and K the thermal conductivity of the particle. For cases where the Biot number is much less than 0.02 (Kuzay *et al.*, 2001), convection is the dominant mechanism and conduction is not significant. Some authors give a cutoff value for the Biot number of 0.1 for assessing the relative importance of heat convection and conduction (Bald, 1987). Assuming a spherical crystal, in combination with the fluid properties of gaseous nitrogen (Wolley, 1956), we calculate an average convection heat-transfer coefficient of $0.013 \text{ W cm}^{-2} \text{ K}^{-1}$ and a volume-equivalent radius of the crystal of 0.032 cm . An estimate of $0.003 \text{ W cm}^{-1} \text{ K}^{-1}$ was obtained from values of thermal conductivity reported for biological materials (Bald, 1987). This provides a Biot number of 0.14. Conduction is a significant factor, as this value is greater than the cutoff value for the Biot number used to assess significance. Therefore, in this particular case, modeling of the temperature profiles needs to take into account both conduction and convection.

5. Future work

The information that we can obtain from this work is limited, mainly because the data are only qualitative. Quantitative data first and

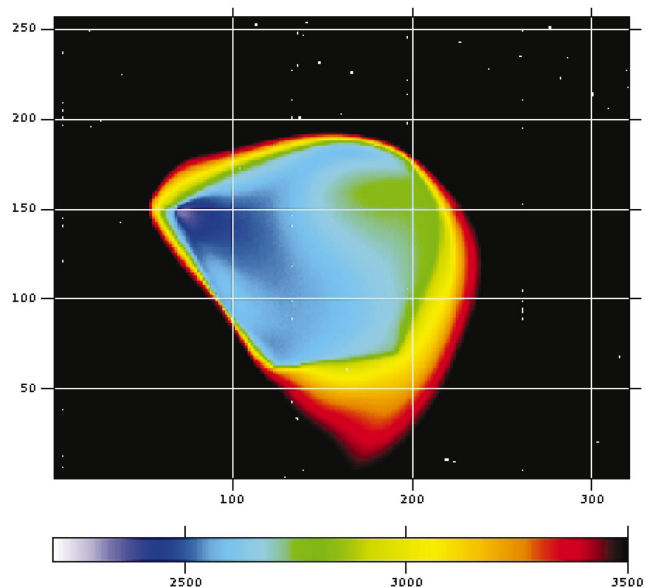


Figure 7

Enlargement of a single frame from Fig. 6. A glucose isomerase crystal, in the absence of a cryoprotectant, shows an S-shaped ‘cold wave’ that progresses through the crystal. This image was recorded approximately 0.03 s after the coldstream was unblocked and allowed to hit the crystal. The false color scheme has been chosen to accent the S-shaped pattern.

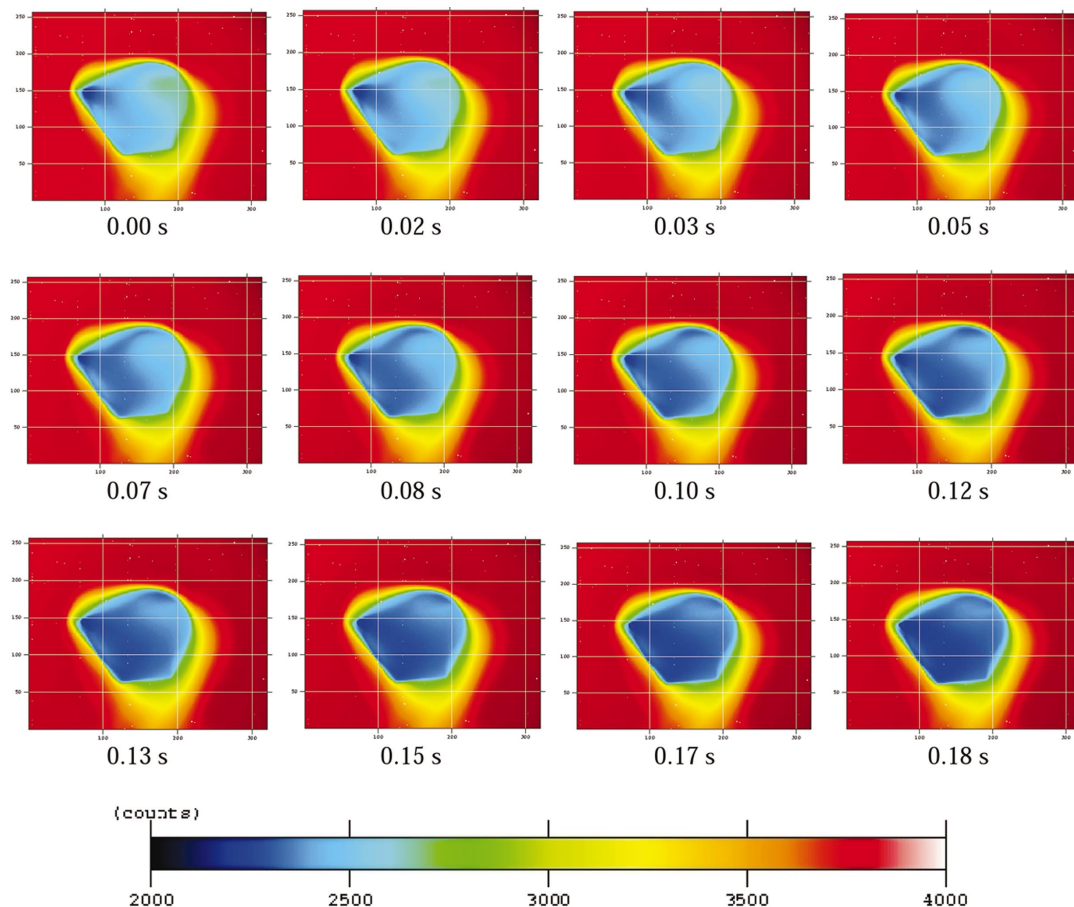


Figure 6

Glucose isomerase cryocooled in the gas stream at 100 K. The imaging was started after unblocking of the coldstream and appears to have captured the cooling shortly after the process has started. The cryostream is positioned identically to that for Figs. 2 and 3.

foremost depend on the ability to calibrate the IR camera, allowing the conversion of intensity values to temperature. The response of the camera to temperature is non-linear, which is corrected with a response function calculated from images of blackbody objects spanning the temperature range to be studied. In this case, blackbodies at ambient temperature and ~ 193 K were available. After correction, the camera response is linear inside this range but deviates at temperatures below 193 K. To calibrate the camera and produce a linear response over the temperatures of interest, a cryogenic blackbody source is needed. With a linear response and a cryogenic blackbody source of known temperature, the camera can accurately measure the temperature of any blackbody over the range of temperatures for which it has been calibrated.

When we establish reasonable estimates for the emissivity constant of a macromolecular crystal at various temperatures, we will be able to accurately assess the temperature distribution in such a crystal. This constant will further increase the reliability of the temperature assigned to a crystal based on the energy emission. With adequate calibration and knowing the emissivity constant, we will be able to estimate thus far unknown values for macromolecular crystals of the thermal diffusivity and the heat capacity. By comparison of cooling data for crystals of different size and habit, we expect to be able to suggest optimal cooling protocols in the future. The development of optimal chemical composition for cryoprotection of macromolecular crystals is a similar obvious target in our future research. Our results pertain to cooling a crystal in a nitrogen gas stream at 100 K. Other methods, such as plunging in a cryogenic liquid or the use of other gasses, are also available. Visualizing the crystal under these different cooling protocols will lead to data on the optimum method for cooling. Finally, we envision a study of a cryocooled crystal while it is irradiated by X-rays from a third-generation synchrotron source. We hope to see the thermal shock caused by the beam and how efficiently heat is removed from the crystal by the cryostream. These data may lead to optimized data-collection protocols, for example, intermittent X-ray exposure per image allowing better heat dissipation than that obtained using a continuous exposure.

6. Conclusions

In this work we show for the first time that it is possible to thermally image macromolecular crystals that are inserted into a nitrogen stream at 100 K. Initial qualitative data clearly show the temperature gradients across the crystal and indicate that a typical cooling time for

a protein crystal inserted into a nitrogen stream is 0.6 s. The experiments also show that it is, in principle, possible to observe defects created by improper cooling, tempering or annealing. Based on the properties of a gaseous nitrogen stream, we estimate the Biot number as ~ 0.14 for the lysozyme crystal in this work. This number indicates that in any modeling study heat transport within the crystal and heat transport at the crystal surface should both be considered. It is likely that neither one can be neglected if we are to explain the cooling process.

Thermal imaging has provided new qualitative information on the cryocooling process. Quantitative information will follow in our future work. Thermal imaging is a completely non-invasive technique suitable for a number of studies. We have proved that not only can we see the heat with an IR camera but also we can clearly see the cold. Infrared imaging provides a powerful new tool for fundamental and practical cryocrystallographic studies.

Dr Henry Bellamy (CAMD) is thanked for useful discussions and application suggestions for this technology. Dr Elspeth Garman (Oxford), James Murray (Oxford), Dr Craig Kundrot (MSFC), Dr Alex Cernov (USRA/MSFC) and Dr Helen Cole (NASA/MSFC) are thanked for useful discussions. This work is funded by NASA NRA awards NAG8-1836 and NCC8-200.

References

- Bald, W. B. (1987). *Quantitative Cryofixation*. Bristol: IOP.
- Dalziel, S. M. (2000). PhD thesis, Chemical Engineering Department, University of Queensland, Brisbane, Australia.
- Garman, E. (1999). *Acta Cryst. D55*, 1641–1653.
- Garman, E. F. & Schneider, T. R. (1997). *J. Appl. Cryst. 30*, 211–237.
- Hudson, R. D. J. (1969). *Infrared System Engineering*. New York: John Wiley and Sons.
- Kazmiecza, M. (2002). Private communication.
- Kuzay, T. M., Kazmiecza, M. & Hsieh, B. J. (2001). *Acta Cryst. D57*, 69–81.
- Otwowski, Z. & Minor, W. (1997). *Methods in Enzymology*, edited by C. W. Carter Jr, pp. 307–326. New York: Academic Press.
- Rodgers, D. W. (1997). *Macromolecular Crystallography Part B*, edited by C. W. J. Carter & R. M. Sweet, pp. 183–203. New York: Academic Press.
- Teng, T. Y. & Moffat, K. (1998). *J. Appl. Cryst. 31*, 252–257.
- Walker, L. J., Moreno, P. O. & Hope, H. (1998). *J. Appl. Cryst. 31*, 954–956.
- Weik, M., Kryger, G., Schreurs, A. M. M., Bouma, B., Silman, I., Sussman, J. L., Gros, P. & Kroon, J. (2001). *Acta Cryst. D57*, 566–573.
- Wolley, H. W. (1956). *Thermodynamic Properties of Gaseous Nitrogen*. Report TN 3271. National Advisory Committee for Aeronautics, USA.